https://doi.org/10.1016/j.ceramint.2021.05.177

Evolution on phase composition and properties of alumina-based ceramics fabricated from high-titania special-grade natural bauxite micropowder

Riqing Du [1], Lvping Fu [1,2,3]*, Huazhi Gu [1], Siu Wing Or [2]*, Ao Huang [1], Renxiang Lv [3], Qiong Luo [4]

[1] The State Key Laboratory of Refractories and Metallurgy, Wuhan University of Science and Technology, Wuhan 430081, China

[2] Department of Electrical Engineering, The Hong Kong Polytechnic University, Hung Hom, Kowloon, Hong Kong

[3] Jinan Ludong Refractories Co., Ltd., Jinan 250109, China

[4] Foshan Ceramics Research Institute Co., Ltd., Foshan 528031, China

*Corresponding author

Abstract

In this study, Al_2O_3-based ceramics were fabricated with natural bauxite powder as the raw material. The phase compositions evolution behavior during the heat treatment and its influence on the properties of fabricated ceramics were investigated. With increasing heat treatment temperature, the sintering degree of high-titania special-grade bauxite became better. The samples showed decreased porosity, increased bulk density, Vickers hardness, fracture toughness and flexural strength. However, when the heat temperature increased to 1650 °C, decomposition of tieillite occurs in sample, leading to increased Al_2O_3 and TiO_2 content in the liquid phase. Corundum and mullite grains with anisotropic growth appeared in the samples, leading

to a decrease in the density, the Vickers hardness and flexural strength of samples decreased consequently. However, those anisotropic grains could prolong the crack propagation path and improve the fracture toughness of the material.

Key words: Al_2O_3-based ceramics; phase compositions; properties; natural bauxite

1. Introduction

Alumina ceramic has been widely used as cutting tools, wear resistant coatings, thermal insulators, dental prostheses and armor systems, because they often have high hardness, good wear resistance, outstanding corrosion resistance and chemical stability [1-8].

Generally, alumina ceramics are produced with industrial alumina as the main raw material [9,10]. During the fabrication of alumina ceramics, in order to reduce the sintering temperature and avoid grain growth, sintering enhancement through the addition of dopants is widely accepted [11-13]. Among varied dopants, TiO_2, SiO_2, MgO and CaO are the most common sintering aids used for alumina ceramics [14-18]. By introducing TiO_2 additive into alumina-based ceramics, Manshor et al. [14] found that the fracture toughness and hardness were enhanced with appropriate TiO_2 addition. Fabris et al. [15] fabricated alumina armors by adding $MgO{\cdot}Al_2O_3{\cdot}SiO_2$ sintering aid, and pointed out that the glass-ceramic addition led to lower sintering time and temperature, the ceramic composites showed ballistic performance equivalent to that of high-purity alumina.

High-titania special-grade bauxite is a widespread natural raw material, whose main chemical composition is Al_2O_3 and TiO_2, as well as small amounts of SiO_2, Fe_2O_3

and CaO. Numerous research works have been performed concerning on the processing and thermal evolution of natural bauxites. The phase equilibrium relationships in the system Al_2O_3-SiO_2-TiO_2-Fe_2O_3 in air was studied by Caballero et al. [19,20], who reported the solubilities of Fe_2O_3 and TiO_2 in mullite and tieillite, which may lead to the refinement of microstructure and densification. They also pointed out that the high-temperature mechanical properties and microstructure of bauxite could be modified by controlling the compositions of second solid phase. Moreover, the solid solutions of TiO_2 into phases of mullite, corundum, spinel have been verified in several research studies, resulting in improved sintering and mechanical properties [21,22]. Therefore, high-titania special-grade bauxite is a potential raw material for the fabrication of alumina ceramic without sintering aids addition. Compared to the industrial alumina ceramics, Al_2O_3-based ceramics from natural bauxite have obvious advantages in low cost and saving energy, and can be used as abrasive materials, refractory materials and proppants.

Consequently, in this study, Al_2O_3-based ceramics are fabricated with natural high-titania special-grade bauxite powder as the raw material. The phase compositions evolution behavior during the heat treatment and its influence on the properties of fabricated ceramics are discussed in detail.

2. Experimental

2.1 Raw materials

High-titania special-grade bauxite micropowder, with a median particle diameter of 3.44 μm, was selected as the raw material in this work. The bauxite micropowder was fabricated from natural high-titania special-grade bauxite powder (<0.088 mm,

Henan Bauxitechina Co., Ltd., Henan, China), which was milled in a planetary ball mill (QM-BP, Nanjing Nanda Instrument Plant, China) for 120 minutes. The planetary ball mill was operated at 365 rpm, and alumina balls of 8-14 mm in diameter were used with a charge ratio of 7:1.

The chemical compositions of high-titania special-grade bauxite are provided in Tables 1. Besides small amounts of SiO_2, Fe_2O_3 and CaO, the high-titania special-grade bauxite consists mainly of alumina and titania, with a Al_2O_3 and TiO_2 total content of 97.83 wt%.

Table 1. Chemical compositions of high-titania special-grade bauxite

Raw materials	Chemical compositions/wt%								
	Al_2O_3	MgO	SiO_2	Fe_2O_3	K_2O	Na_2O	TiO_2	CaO	IL
Original composition	79.71	0.11	0.72	0.39	0.01	0.01	3.99	0.37	14.45
Composition without IL	93.17	0.13	0.84	0.46	0.01	0.01	4.66	0.43	-

The phase compositions of high-titania special-grade bauxite raw material is given in Fig. 1 (a), diapore is the primary phase, while the peak of anatase phase has also been detected. As for the TG and DSC traces of bauxite given in Fig. 1 (b), a weight loss of approximately 16 % was measured from 25 °C to 1500 °C. The weight-loss region from room temperature to around 400 °C is attributed to the removal of physically absorbed water. Due to the eliminating of immobilized water in diaspore, a large weight-loss was detected in the temperature range of 450–550 °C. One endothermic peak, around 505.1 °C, was observed, which is caused by the water removal of weight-loss diaspore.

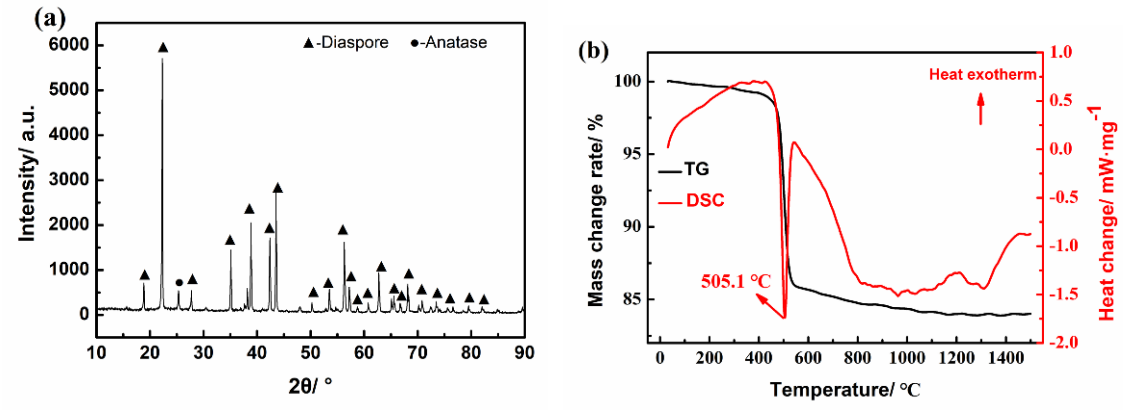

Fig. 1. (a) XRD pattern and (b) TG-DSC traces of bauxite raw material

2.2 Sample preparation

With 1 wt% polyethylene glycol as binder, high-titania special-grade bauxite micropowder and the binder were mixed uniformly in a planetary ball mill (QM-BP, Nanjing Nanda Instrument Plant, China) for 30min. The mixture was uniaxially pressed into green bodies at a pressure of 150 MPa. After drying at 80 ℃ and 110 ℃ for 24 hours respectively, the green bodies were heated at different temperatures for 3 hours in an electric furnace (SK17-4-3, Luoyang Precondar Instruments for Testing Refractoriness Co., Ltd., Henan, China). In this study, the heat treatment temperatures were set as 1500 ℃, 1550 ℃, 1600 ℃, 1650 ℃ and 1700 ℃, respectively. The samples were heated at a rate of 5 ℃/min from room temperature to 1000 ℃, at a rate of 3 ℃/min from 1000 ℃ to 1400 ℃, and then 1 ℃/min from 1400 ℃ to the final temperature.

2.3 Testing and characterization

As shown in Eq. (1), the height of samples before and after sintering (h and h_s) were measured to determined the linear shrinkage (L). Using water as medium, the

bulk density (ρ_b) and open porosity (π_o) of samples were measured based on the Archimedes' Principle. After being milled into 325 mesh-sieved powders, the true density (ρ_t) of the sample was determined using an automatic true density analyzer (Accupyc 1330, Micromeritrics Instrument Corporation, Norcross, USA). Then the total pororsity (π_t) and closed porosity (π_c) of samples were calculated from true densities and bulk densities according to Eqs. (2) and (3). In this study, ten determinations were performed for the measurement of linear shrinkage, bulk density, open porosity, and true density of each sample.

$$L = \frac{h_s - h}{h} \times 100 \tag{1}$$

$$\pi_t = \frac{\rho_t - \rho_b}{\rho_t} \times 100\% \tag{2}$$

$$\pi_c = \pi_t - \pi_o \tag{3}$$

Phase identification is carried out by means of an X-ray diffractometer(Panalytical, X'Pert Pro MPD, Netherlands) where patterns were recorded using a Cu radiation(λ =0.1542 nm) with a scanning rate of 2°/min from range of 10° to 90°. Celref calculation software (Beta Version 2000, Grenoble INP, France) was used to refine the XRD patterns of different samples, and the lattice constants of corundum and mullite phases in different samples were measured. The microstructure and element distribution of specimen were analyzed by a field emission scanning electron microscope (FESEM, Quanta 400, FEI Company, USA) equipped with an energy dispersive X-ray spectrometer (EDX, QUANTAX, Bruker, Berlin, Germany) according to ISO 22309:2006.

The Vickers hardness indentations were made on polished sample surface by a Vickers hardness tester (HV-50A, Laizhou Huayin Testing Instrument Co., Ltd., China)

equipped with a diamond pyramid indenter, applying a load of 5 kg and a loading time of 10 s. Three-point flexural strength test was carried out on the samples (3 mm×4 mm×36 mm) using a universal testing machine (ETM1050, Shenzhen Wance Testing Machine Co., Ltd., Guangdong, China) with a span of 30 mm. After being cut into size of 3 mm×4 mm×45 mm, fracture toughness was measured using single edge notched beams (SENB) method using the above-mentioned universal testing machine with a span of 40 mm. To guarantee the accuracy of the experimental results, ten determinations were conducted for the measurement of mechanical properties of each sample.

2.4 Thermodynamic calculations

In order to clarify the phase compositions evolution of high-titania super-grade bauxite at different heat treatment temperatures, thermodynamic calculations were carried out to predicted the equilibrium phases of samples. According to the chemical compositions of high-titanium super-grade bauxite shown in Table 1, the expected equilibrium phases of samples in the experimental temperature range (1500 °C-1700 °C) were calculated by using the 'Equilibrium' module of FactSage 6.4. During the thermodynamic calculations, the databases of FToxid 6.4 and FactPS 6.4 were selected.

3. Results and Discussion

3.1 Phase composition

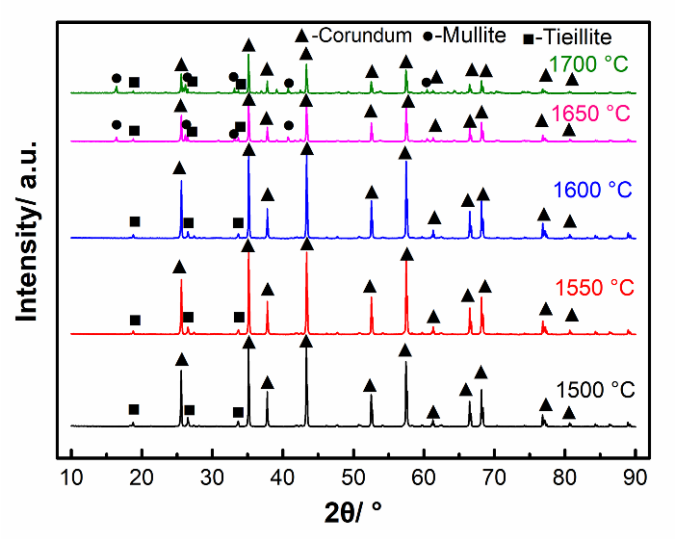

Fig. 2. XRD patterns of samples after different heat treatment temperatures

Fig. 2 provides the XRD patterns of samples heated at different temperatures. For the samples heated at 1500 ℃, 1550 ℃, 1600 ℃, the main crystalline phase was corundum, and secondary crystalline phase, tieillite (Al_2TiO_5), was also detected. As the heat treatment temperature increased to 1650 ℃, mullite ($3Al_2O_3{\cdot}2SiO_2$) phase peaks appeared in the samples. In this case, the main crystalline phase was still corundum (α-Al_2O_3), apart form that, some tieillite and mullite phases were found.

Table 2 provides the quantitative study of various samples. With the increasing heat treatment temperature, the intensity associated with tieillite phase decreased gradually, indicating a reduction in content of tieillite phase. However, with the heat treatment temperature increased from 1650 ℃ to 1700 ℃, the peak intensity of mullite increased. It can be infered that with the increase of heat treatment temperature, the

decomposition of tieillite phase might occur [23], promoting the reaction between SiO_2 and Al_2O_3, consequently leading to the formation and crystallization of mullite phase.

Table 2. Phase compositions in various samples

Heat treatment temperature/ ℃	Corundum	Tieillite	Mullite	Vitreous phase
1500	89	5	-	6
1550	87	5	-	8
1600	88	4	-	8
1650	74	3	11	12
1700	62	3	21	14

The lattice constants of corundum and mullite phases in different samples were shown in Table 3, in the temperature range from 1500 ℃ to 1600 ℃, the lattice constants of the corundum phase changed slightly. However, as the heat treatment increased to 1650 ℃ and 1700 ℃, the lattice constants of corundum and mullite phase both increased significantly. It has been reported that TiO_2 could dissolve into mullite solid solution by replacing Al^{3+} or Si^{4+} with Ti^{4+} [24]. According to the ion radius of Si^{4+} (0.026 nm), Al^{3+} (0.053 nm) and Ti^{4+} (0.061 nm), replacement of Al^{3+} by Ti^{4+} is easier to occur, leading to the formation of $Ti_{Al}^{\square}$ and $o_i^{''}$. That makes the lattice constant of mullite solid solution increases, resulting in lattice distortion and anisotropic growth of mullite grains.

Table 3. Lattice parameters of corundum and mullite in various samples

Heat treatment	Corundum			Mullite		
temperature/ ℃	a/ Å	b/ Å	c/ Å	a/ Å	b/ Å.	c/ Å
1500	4.7598	4.7598	12.9931	-	-	-
1550	4.7598	4.7598	12.9934	-	-	-
1600	4.7596	4.7596	12.9933	-	-	-
1650	4.7611	4.7611	12.9947	7.5820	7.6895	2.8941
1700	4.7609	4.7609	12.9948	7.5903	7.6972	2.8934

The predicted equilibrium phases of samples at different temperatures by Fact Sage 6.4 are shown in Fig. 3.

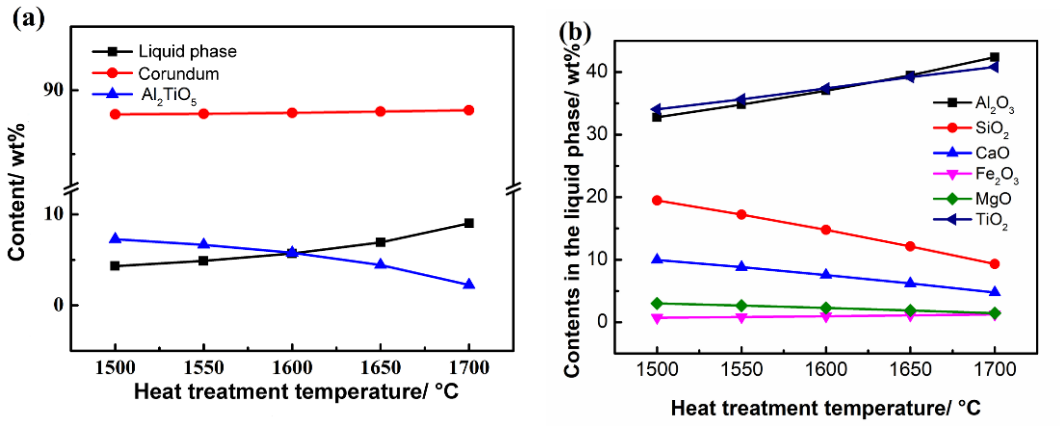

Fig. 3. Predicted phase compositions of samples at different temperatures: (a) predicted phase compositions; (b) compositions in liquid phase

As shown in Fig. 3 (a), in the temperature range from 1500 °C to 1700 °C, the phase compositions of samples were corundum solid phase, tieillite solid phase and high-temperature liquid phase. Compared with the XRD results of samples, no mullite phase was found in the thermal calculations. This may be caused by two reasons. Firstly, it should be pointed out that a small amount of TiO_2, Fe_2O_3 and SiO_2, approximately 0.5 wt%, were detected in the solid phase of corundum. That indicates the possibility of tieillite and mullite solid solution in corundum phase. Secondly, this may be because only thermodynamic factors were considered during the thermodynamic calculations, while the dynamic factors of the crystallization and growth of mullite phase were not included. In addition, what the thermal calculation predict is the phase compositions at high temperature, while the XRD test is carried out on the cooled-samples (crystallization may occur during the cooling process).

With the increasing of temperature, the contents of corundum phase almost kept unchanged, while the tieillite contents decreased gradually, and the liquid phase

contents increased accordingly (Fig. 3 (a)). According to the contents of each component in the liquid phase shown in Fig. 3 (b), the contents of Al_2O_3 and TiO_2 in the liquid phase increased significantly with the increase of temperature. Therefore, it can be inferred that with the increasing temperature, the decomposition of tieillite phase would occur, resulting in increased contents of Al_2O_3 and TiO_2 components in the liquid phase.

3.2 Microstructure

The SEM images of the samples heated at different temperatures are shown in Fig. 4.

When the heat treatment temperature was 1500 ℃, numerous intercrystalline pores, with sizes of about 3-10 μm, were observed in the sample (Figs. 4 (a)-(b)), indicating that a low sintering degree and bonding between grains. The energy spectrum results in Table 4 show that the titania component in the sample mainly existed in the form of tieillite and distributed between corundum particles, which is consistent with the XRD results. As confirmed by the energy spectrum results, a small amount of TiO_2, Fe_2O_3 and SiO_2 were dissolved in the corundum grains, indicating the solid solution of tieillite and mullite in corundum phase. The ternary equilibrium phase diagram of Al_2O_3-SiO_2-TiO_2 system has been investigated by Caballero et al. [19,20], who pointed out that possibility of mullite in corundum, which is also in agreement with the thermodynamic calculation results.

As the heat treatment temperature increased to 1550 ℃, the number of pores in the sample decreased significantly and the compact level increased (Figs. 4 (c)-(d)). With the heat treatment temperature being further raised to 1600 ℃, the porosity was

continued decreased, the sample has a good sintering degree and a dense structure (Figs. 4 (e)-(f)). As shown in Table 4, in the temperature range from 1500 ℃ to 1600 ℃, no significant change was found in the phase compositions of the samples, remaining being composed of corundum and tieillite phases. The corundum particles were granular, while tieillite particles were distributed between corundum particles.

However, as the heat treatment temperature increased to 1650 ℃, several large pores were observed in the sample, and the density decreased instead (Fig. 4 (g)). Higher magnification SEM image suggested that numerous platelike and elongated grains were formed in the sample (Fig. 4 (h)). The results of energy spectrum analysis in Table 4 indicated that the platelike and elongated grains were mainly corundum grains. Besides, some acicular and elongated mullite grains were also detected (Fig. 4 (h)). Due to the formation of corundum and mullite grains with anisotropic growth, the sintering and densification of the samples became more difficult. As shown in Fig. 4 (h), attributing to the staggered distribution of those anisotropic-grew grains, numerous pores had been produced around them, leading to decreased density of the sample. Fig. 4 (i) provided the SEM images of precipitated mullite phase in the sample heated at 1650 ℃. TiO_2 components (red arrows) filled in the gaps among the columnar mullite grains (white arrows). Several published works have pointed out that the introduction of TiO_2 into a high-temperature aluminum-silicate liquid phase would reduce the liquid viscosity, promoting the precipitation and nucleation of mullite [24-26]. In addition, the formation of mullite is controlled by the solution-precipitation reaction, increased Al_2O_3 content in the liquid phase will also make the precipitation of mullite becomes easier. As the thermodynamic calculations results shown in Fig. 3, with the increasing heat treatment temperature, the contents of Al_2O_3 and TiO_2 in the liquid phase

increased, consequently promoting the formation of mullite phase. Additionally, co-doping of TiO_2 and SiO_2 result in the formation of ternary eutectic liquid phase around the alumina grains, promoting the abnormal growth of the alumina grains into plate-shaped and columnar anisotropic grains [27].

With the heat treatment temperature increased to 1700 ℃, the number of anisotropic grains in the samples further increased (Fig. 4 (j)). In addition, the content of mullite grains in the samples increased accordingly (Fig. 4 (k)). It is worthy to pointed out that the results of energy spectrum analysis suggested there was a certain amount of TiO_2 in the solid solution of mullite [19,20].

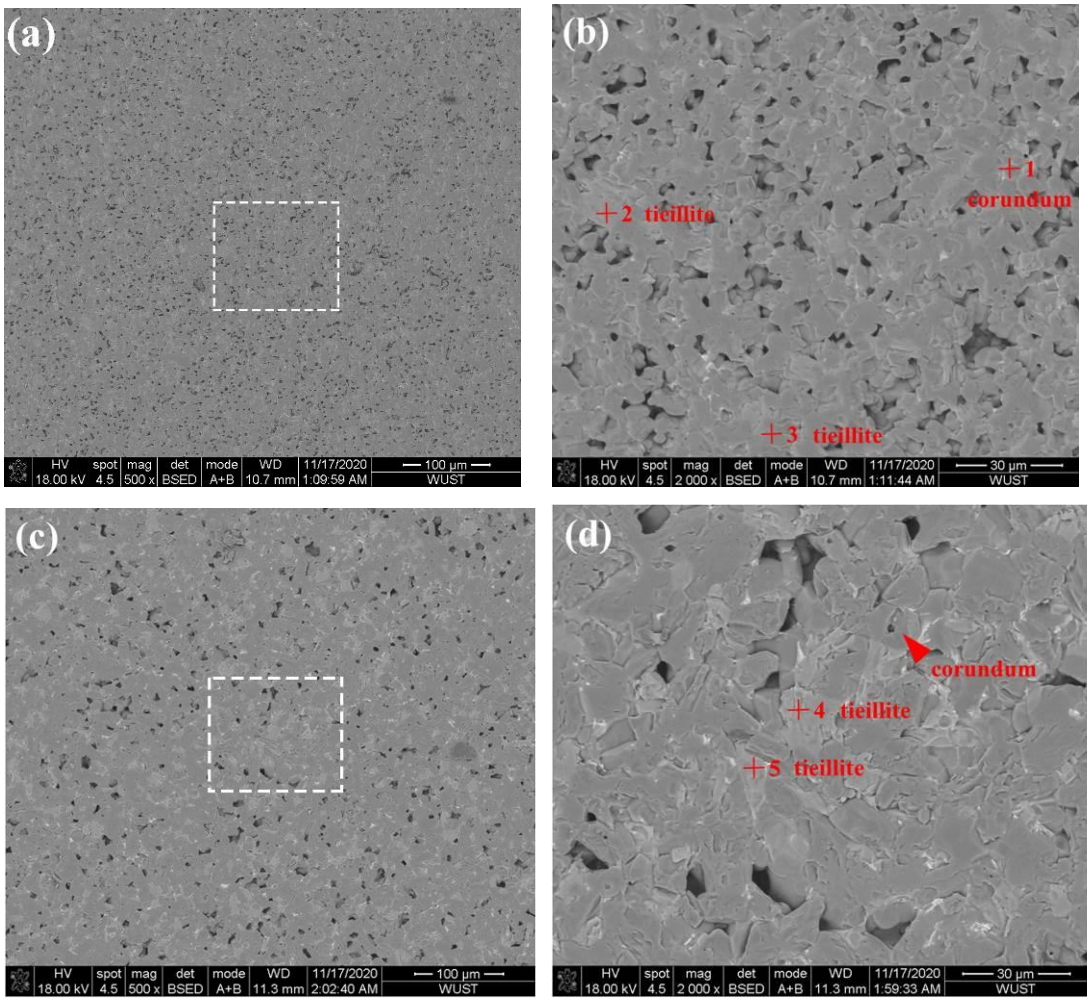

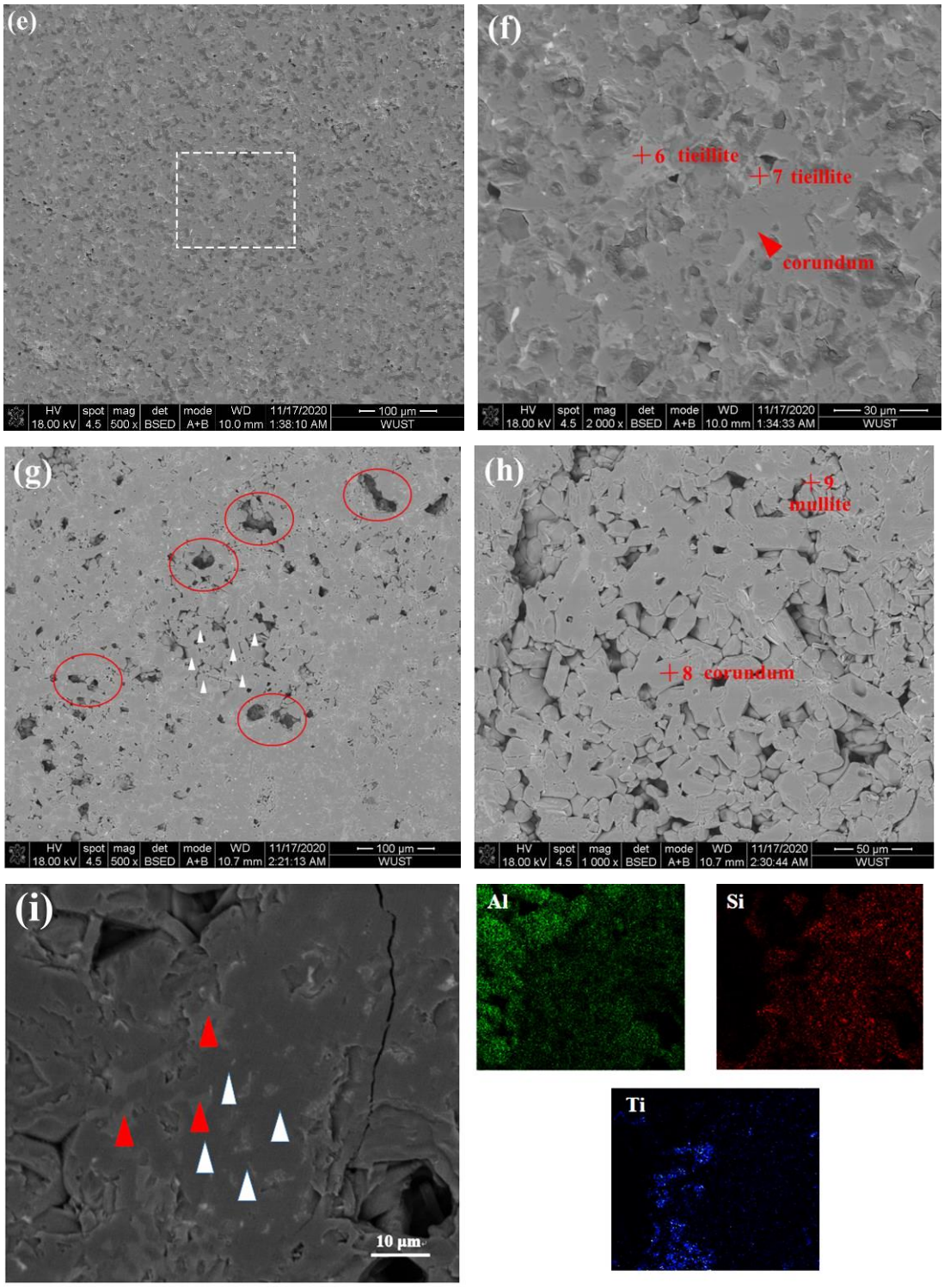
(e)
HV 18.00 kV | spot 4.5 | mag 500 x | det BSED | mode A+B | WD 10.0 mm | 11/17/2020 1:38:10 AM | 100 µm | WUST
(f)
+6 tieillite
+7 tieillite
corundum
HV 18.00 kV | spot 4.5 | mag 2 000 x | det BSED | mode A+B | WD 10.0 mm | 11/17/2020 1:34:33 AM | 30 µm | WUST
(g)
HV 18.00 kV | spot 4.5 | mag 500 x | det BSED | mode A+B | WD 10.7 mm | 11/17/2020 2:21:13 AM | 100 µm | WUST
(h)
+9 mullite
+8 corundum
HV 18.00 kV | spot 4.5 | mag 1 000 x | det BSED | mode A+B | WD 10.7 mm | 11/17/2020 2:30:44 AM | 50 µm | WUST
(i)
10 µm
Al
Si
Ti

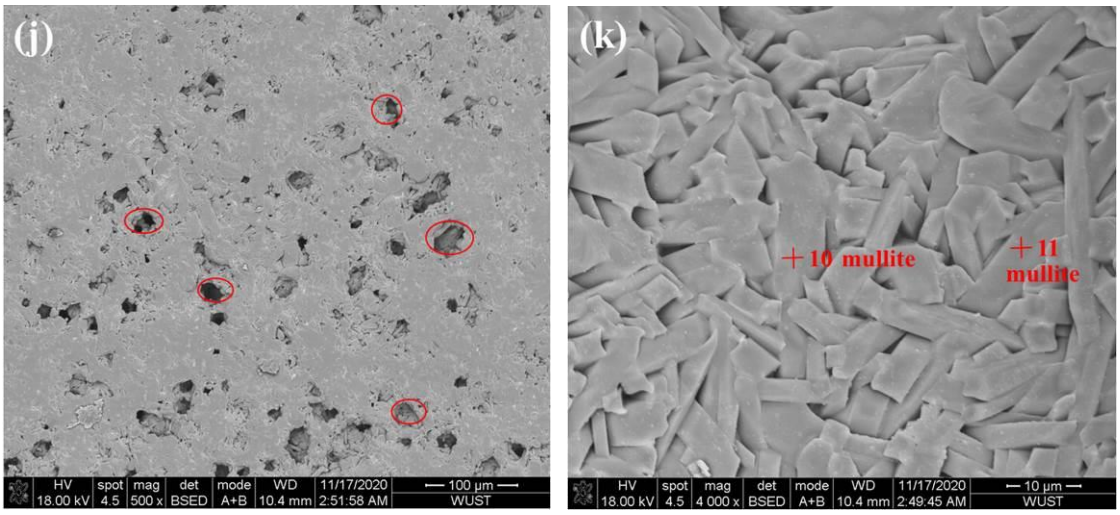

Fig. 4. SEM images of samples heated at different temperatures: (a)-(b) 1500 °C; (c)-(d) 1550 °C; (e)-(f) 1600 °C; (g)-(i) 1650 °C; (j)-(k) 1700 °C

Table 4. Energy dispersive analyses of various samples

Points	Ti/ wt%	Al/ wt%	Si/ wt%	O/ wt%	Fe/ wt%	Possible phase
1	0.4±0.2	59.1±0.5	2.0±0.3	37.7±1.0	0.8±0.3	corundum
2	27.2±0.5	28.9±0.4	-	44.0±1.5	-	tieillite
3	26.8±0.5	30.1±0.4	-	43.1±1.5	-	tieillite
4	34.3±0.6	31.8±0.4	-	33.9±1.7	-	tieillite
5	30.0±0.7	30.5±0.5	-	39.5±2.1	-	tieillite
6	29.9±0.6	29.8±0.5	-	40.2±1.9	-	tieillite
7	29.7±0.6	30.3±0.5	-	40.0±2.0	-	tieillite
8	-	62.9±0.6	-	37.1±1.1	-	corundum
9	1.8±0.3	39.7±0.7	10.8±0.5	47.7±1.6	-	mullite
10	3.6±0.3	44.1±0.5	13.9±0.4	38.4±1.1	-	mullite
11	3.9±0.3	44.3±0.5	15.0±0.4	36.8±1.2	-	mullite

3.3 Sintering properties

Fig. 5 shows the sintering properties of samples heated at different temperatures. For the sample heated at 1500 ℃, it had a bulk density of 3.46 g/cm^3 and an open porosity up to 7.6%, indicating a dissatisfied sintering degree. With the heat treatment temperature gradually increased from 1500 ℃ to 1550 ℃ and 1600 ℃, due to the improved sintering densification degree, the linear shrinkage and bulk density of the

samples increased, while the total porosity gradually decreased. When the sintering temperature was 1600 ℃, the sample exhibited the best sintering degree, had a bulk density as well ad total, closed and open porosity of 3.71 g/cm^3, 2.8%, 2.7%, and 0.1%, respectively.

However, with the heat treatment temperature further increased to 1650℃, numerous staggered distributed corundum and mullite grains with anisotropic growth were formed in the samples (Fig. 4 (h)). As a result, the sintering densification of sample became difficult, leading to decreased linear shrinkage and bulk density, and increased total porosity. As the heat treatment temperature increased to 1700 ℃, the bulk density and linear shrinkage of the samples further decreased, while the total and closed porosity continued to increase.

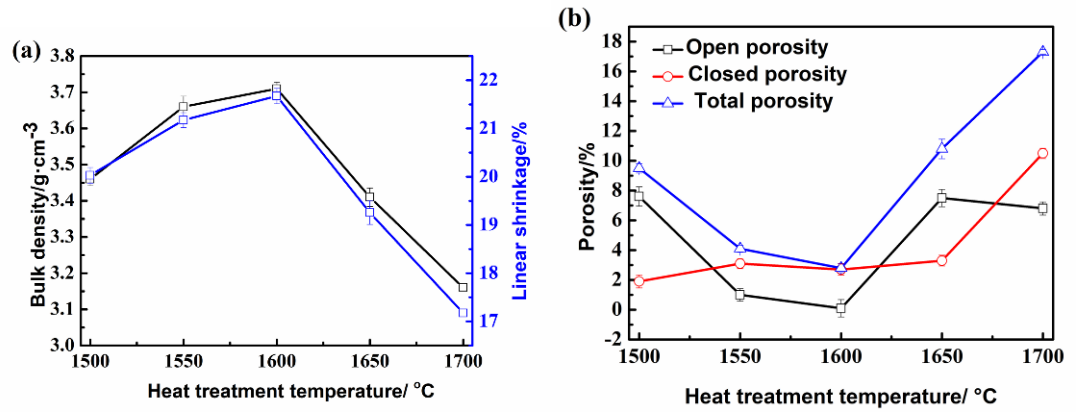

Fig. 5. Properties of samples heated at different temperatures: (a) densities and linear shrinkages; (b) porosities

3.4 Mechanical properties

The mechanical properties of samples heated at different temperatures are shown in Fig. 6.

The Vickers hardness exhibited coincident trend with the bulk density of samples. With the heat treatment temperature increased from 1500 ℃ to 1550 ℃ and 1600 ℃, the Vickers hardness of the samples gradually increased, which is mainly due to the improved sintering densification of samples. However, as the heat treatment temperature further increased to 1650 ℃ and 1700 ℃, the Vickers hardness decreased instead. This is because the increase in porosity of samples (Figs. 4 (g)-(k)), which has a negative impact on the hardness of materials. After heated at 1600 ℃, the sample has the highest Vickers hardness, at 11.2 GPa.

In terms of fracture toughness and flexural strength, they both increased at first and then decreased, with the increase of heat treatment temperature. As the heat treatment temperature increased from 1500 ℃ to 1550 ℃ and 1600 ℃, the fracture toughness and flexural strength of the samples were improved. Unlike Vickers hardness, fracture toughness is further increased when the heat treatment temperature was increased from 1600 ℃ to 1650 ℃. This may be mainly due to the formation of numerous anisotropic corundum and mullite grains in the sample, which could improve the toughness of the materials. However, the flexural strength was slightly reduced instead. With the heat treatment temperature further increased to 1700 ℃, the fracture toughness and flexural strength decreased due to the increased intergranular porosity of sample. The sample heated at 1650 ℃ exhibited a highest fracture toughness of 6.07 MPa $m^{1/2}$, while the sample treated at 1600 ℃ showed an optimal flexural strength of 312 MPa.

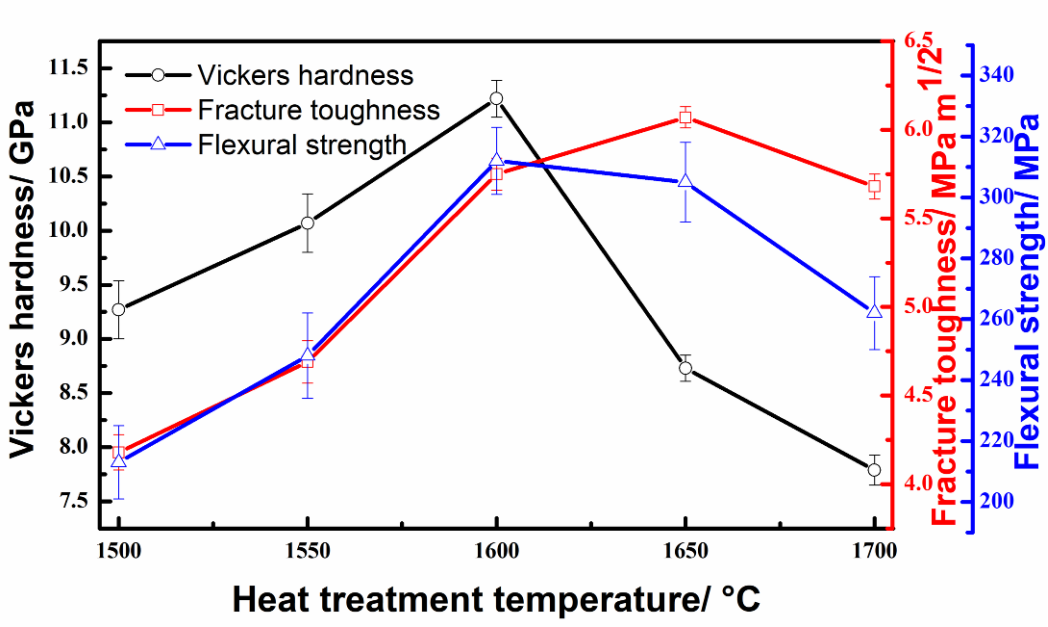

Fig. 6. Mechanical properties of samples heated at different temperatures

SEM images of fracture of different samples are provided in Fig. 7. After heated at 1500 ℃, the sample exhibited a small grain size of approximately 5-10 μm (Fig. 7 (a)), and numerous pores were observed among the grains, indicating an unsatisfied sintering densification. In this case, the fracture mode of the sample was mainly intergranular fracture, while fewer transgranular fractures were observed (red arrow in the figure). As the heat treatment temperature increased to 1550 ℃ and 1600 ℃, the grain sizes gradually increased to 10-20 μm, while the porosity in the samples decreased. The proportions of transgranular fracture increased (Figs. 7 (b)-(c)). Elongated columnar grains were observed in the samples heated at 1650 ℃, and transgranular fracture of columnar grains could be found in the fracture surface (Fig. 7 (d)). When the heat treatment temperature further increased to 1700 ℃, the sizes of anisotropic grains in the sample further increased (Fig. 7 (e)).

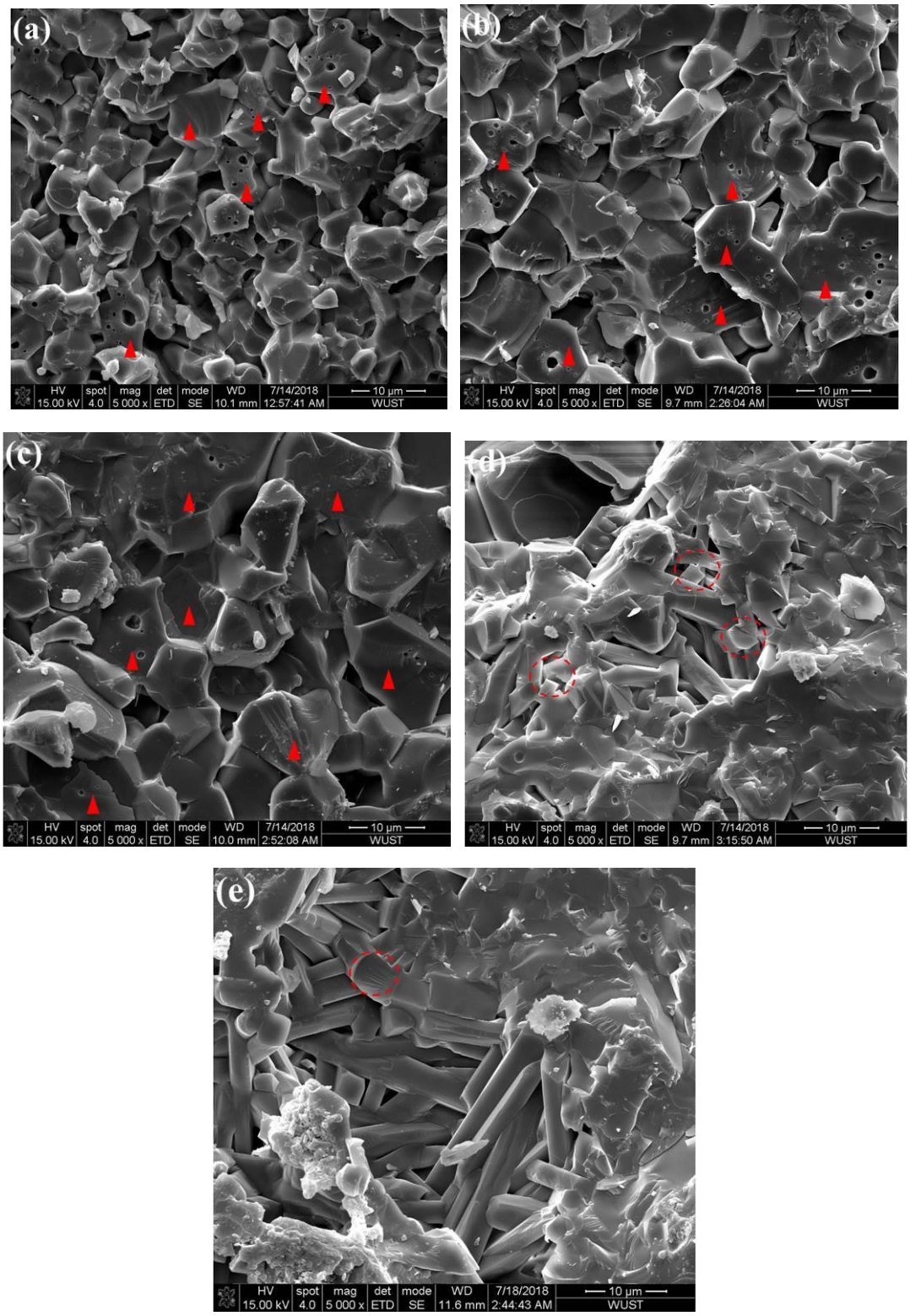

Fig. 7 Fracture surfaces of samples heated at different temperatures: (a) 1500 ℃; (b) 1550 ℃; (c) 1600 ℃; (d) 1650 ℃; (e) 1700 ℃

Numerous studies have been conducted on the impact of anisotropic grains on the mechanical properties of alumina ceramics [28,29]. As shown in Fig. 8, the existence of anisotropic grains could prolong the crack propagation path, and there were crack propagation forms such as transgranular, bridging and deflection. Fracture energy would be absorbed and consumed by crack transgranular and deflection, while crack bridging could further disperse the crack propagation energy and reduce the stress intensity factor and stress concentration at the crack tip. Therefore, the driving force of crack propagation was greatly reduced, resulting in improved fracture toughness.

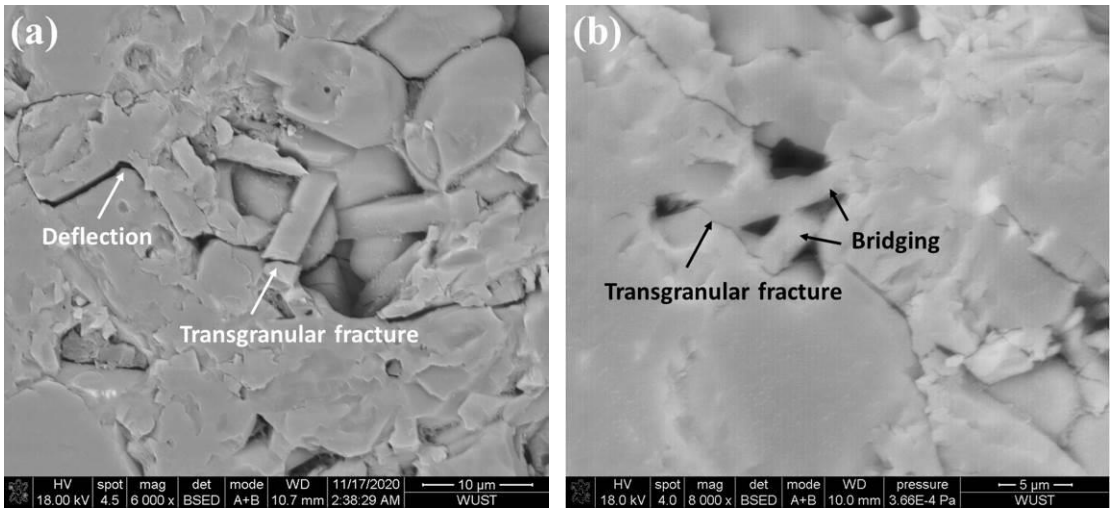

Fig. 8 Effect of anisotropic grain on the crack propagation of samples: (a) deflection and transgranular fracture; (b) bridging and transgranular fracture

In summary, the influence of heat treatment temperature on the mechanical properties of the samples can be deduced. When being heated at 1500 ℃, the sample exhibited unsatisfied sintering densification, the fracture mode of the sample was mainly intergranular fracture, showing relatively low Vickers hardness and fracture toughness. As the heat treatment temperature increased to 1550 ℃ and 1600 ℃, due to the improved sintering densification degree, the density of samples increased. The Vickers hardness and the transgranular fracture proportion increased, resulting in

improved fracture toughness. With the heat treatment temperature further increased to 1650 ℃, corundum and mullite grains with anisotropic growth appeared in the samples, leading to a decrease in the density, the Vickers hardness and flexural strength of samples decreased consequently. However, those anisotropic grains could prolong the crack propagation path and improve the fracture toughness of the material. As the heat treatment temperature increase to 1700 ℃, the sample showed a further decreased density, hardness and fracture toughness. The sample heated at 1600 ℃ exhibited the best comprehensive mechanical properties, had a Vickers hardness, fracture toughness and flexural strength of 11.2 GPa, 6.05 MPa $m^{1/2}$ and 312 MPa, respectively.

In order to assess the potential application possibility of alumina ceramics fabricated from natural bauxite, a comparation on the properties of the ceramics prepared by industrial alumina in other studies and by natural bauxite in this work has been provided in Table 5. Although the bauxite-based alumina ceramic showed a lower flexural strength than the alumina ceramics prepared by industrial alumina, a flexural strength of 312 MPa is high enough for most applications field. Meanwhile, a significantly improvement has been found in the fracture toughness when using the natural bauxite raw material.

Table 5. Properties of different alumina ceramics

References	Sintering temperature / ℃	Vickers hardness/GPa	Fracture toughness/MPa $m^{1/2}$	Flexural strength/MPa
[29]	-	-	4.9	440
[30]	1600	9.5	-	480
[30]	1500	20	4.1	578
[31]	1550	-	3.8	325
This work	1600	11.2	6.05	312

5. Conclusions

(1) In the heat treatment temperature range from 1500 ℃ to 1600 ℃, the sintered samples are mainly composed of corundum and tieillite. With the increasing heat treatment temperature, the samples exhibit improved sintering densification and Vickers hardness, while the porosity decreases. The transgranular fracture proportions increase, resulting in improved fracture toughness and flexural strength.

(2) When the heat treatment temperature increases to 1650 ℃, decomposition of tieillite occurs in sample, leading to increased Al_2O_3 and TiO_2 content in the liquid phase. The precipitation and formation of mullite phase and the anisotropic growth of corundum grains are promoted. Corundum and mullite grains with anisotropic growth appeared in the samples, leading to a decrease in the density, the Vickers hardness and flexural strength of samples decreased consequently. However, those anisotropic grains could prolong the crack propagation path and improve the fracture toughness of the material. As the heat treatment temperature increase to 1700℃, the sample showed a further decreased density, hardness and fracture toughness.

(3) The sample heated at 1600 ℃ exhibited the best comprehensive mechanical properties, had a Vickers hardness, fracture toughness and flexural strength of 11.2 GPa, 6.05 MPa $m^{1/2}$ and 312 MPa, respectively. Compared to the alumina ceramics prepared by industrial alumina, the bauxite-based alumina ceramic showed lower flexural strength, similar Vickers hardness and significantly improved fracture toughness.

Acknowledgements

The authors are thankful for the financially support from the National Natural

Science Foundation of China (Grant No. 51802231), the Hong Kong Scholars Program 2020 (Grant No. G-YZ4E/ XJ2020023), the China Postdoctoral Science Foundation (Grant No. 2017M622535) and the WUST National Defence Pre-research Foundation (Grant No. GF201905).

References

[1] M. Schwentenwein, J. Homa, Additive manufacturing of dense alumina ceramics, Int. J. Appl. Ceram. Tec. 12 (2015) 1-7. https://doi.org/10.1111/ijac.12319

[2] J. Jiusti, E.H. Kammer, L. Neckel, N.J. Lóh, W. Trindade, A.O. Silva, O.R.K. Montedo, A.D. Noni, Ballistic performance of Al_2O_3 mosaic armors with gap-filling materials, Ceram. Int. 43 (2017) 2697–2704. https://doi.org/10.1016/j.ceramint.2016.11.087

[3] L.P. Fu, H.Z. Gu, A. Huang, H.W. Ni, Correlations among processing parameters and porosity of a lightweight alumina, Ceram. Int. 44 (2018) 14076–14081. https://doi.org/10.1016/j.ceramint.2018.05.005

[4] L.P. Fu, H.Z. Gu, A. Huang, Y.S. Zou, M.J. Zhang, Fabrication of lightweight alumina with nanoscale intracrystalline pores, J. Am. Ceram. Soc. 103 (2018) 2262–2271. https://doi.org/10.1111/jace.16914

[5] O. L. Ighodaro, O.I. Okoli, Fracture Toughness Enhancement for Alumina Systems: A Review, Int. J. Appl. Ceram. Tec. 5 (2008) 313-323. https://doi.org/10.1111/j.1744-7402.2008.02224.x

[6] J.J. Liu, B. Ren, Y.J. Lu, X.Q. Xi, Y.J. Li, K.L. Liu, J.L. Yang, Y. Huang, Novel design of elongated mullite reinforced highly porous alumina ceramics using carbonized rice husk as pore-forming agent, Ceram. Int. 45 (2019) 13964–13970. https://doi.org/10.1016/j.ceramint.2019.04.095

[7] Y. Yin, B.Y. Ma, C.B. Hu, G. Q. Liu, H.X. Li, C. Su, X.M. Ren, J.Y. Yu, Y.R. Zhang, J.K. Yu, Preparation and properties of porous SiC-Al_2O_3 ceramics using coal ash, Int. J. Appl. Ceram. Tec. 16 (2019) 23-31. https://doi.org/10.1111/ijac.13080

[8] X.M. Ren, B.Y. Ma, Y.R. Zhang, D.X. Li, Q. Zhu, L. Yuan, J.K. Yu, G.Q. Liu, H.X. Li, Effects of sintering temperature and V_2O_5 additive on the properties of SiC-Al_2O_3 ceramic foams, J. Alloy. Compd. 732 (2018) 716-724. https://doi.org/10.1016/j.jallcom.2017.10.170

[9] Q. Ren, Y.H. Ren, X.L. Wu, W.N. Bai, J.L. Zheng, O. Hai, Effects of pyrolusite and dolomite co-additives on the structure and properties of bauxite-based ceramics, Mater. Chem. Phys. 230 (2019) 207-214. https://doi.org/10.1016/j.matchemphys.2019.03.072

[10] P. Tan, P. Wu, L. Gao, Y.D. Sui, Y.H. Jiang, Influence of Si_3N_4 content on the physical and mechanical properties of zirconia-toughened alumina (ZTA) ceramic composites, Mater. Res. Express. 6 (2019) 065205. https://doi.org/10.1088/2053-1591/ab0e54

[11] E. Keramat, B. Hashemi, Modelling and optimizing the liquid phase sintering of alumina/CaO–SiO_2–Al_2O_3 ceramics using response surface methodology, Ceram. Int. 47 (2021) 3159–3172. https://doi.org/10.1016/j.ceramint.2020.09.153

[12] H.Y. Li, X.A. Xi, J. Ma, K.H. Hua, A. Shui, Low-temperature sintering of coarse alumina powder compact with sufficient mechanical strength, Ceram. Int. 43 (2017) 5108–5114. https://doi.org/10.1016/j.ceramint.2017.01.024

[13] G.H. Fan, Y.P. Zhao, J.H. Xin, Z.D. Zhang, P.T. Xie, C.B. Cheng, Y.P. Qu, Y. Liu, K. Sun, R.H. Fan, Negative permittivity in titanium nitride-alumina composite for functionalized structural ceramics, J. Am. Ceram. Soc. 103 (2020) 403–411. https://doi.org/10.1111/jace.16763

[14] H. Manshor, S.M. Aris, A.Z. A. Azhar, E.C. Abdullah, Z.A. Ahmad, Effects of TiO_2 addition on the phase, mechanical properties, and microstructure of zirconia-toughened alumina ceramic composite, Ceram. Int. 41 (2015) 3961–3967. https://doi.org/10.1016/j.ceramint.2014.11.080

[15] D.C.N. Fabris, M. B. Polla, J. Acordi, A.L. Luza, A.M. Bernardin, A.D. Noni, O.R.K. Montedo, Effect of $MgO{\cdot}Al_2O_3{\cdot}SiO_2$ glass-ceramic as sintering aid on properties of alumina armors, Mater. Sci. Eng. A. 781 (2020) 139237. https://doi.org/10.1016/j.msea.2020.139237

[16] R. Sarkar, G. Bannerjee, Effect of addition of TiO_2 on reaction sintered $MgO–Al_2O_3$ spinels, J. Eur. Ceram. Soc. 20 (2000) 2133–2141. https://doi.org/10.1016/S0955-2219(00)00097-2

[17] A. Ullah, H.X. Liu, H. Hao, J. Iqbal, Z.H. Yao, M.H. Cao, Influence of TiO_2 additive on sintering temperature and microwave dielectric properties of $Mg_{0.90}Ni_{0.1}SiO_3$ ceramics, J. Eur. Ceram. Soc. 37 (2017) 3045–3049. https://doi.org/10.1016/j.jeurceramsoc.2017.03.047

[18] A. Kebbede, J. Parai, A.H. Carim, Anisotropic grain growth in α-Al_2O_3 with SiO_2 and TiO_2 additions, J. Am. Ceram. Soc. 83 (2000) 2845–2851. https://doi.org/10.1111/j.1151-2916.2000.tb01642.x

[19] A. Caballero, F.J. Valle, S.D. Aza, S. Castillo, Constitution of calcined refractory-grade bauxites: An interpretation, Ceram. Int. 11 (1985) 45-50. https://doi.org/10.1016/0272-8842(85)90008-2

[20] A. Caballero, J. Requena, S.D. Aza, Refractory bauxites. How processing can improve high temperature mechanical properties, Ceram. Int. 12 (1986) 155-160. https://doi.org/10.1016/0272-8842(86)90038-6

[21] R. Naghizadeh, H.R. Rezaie, F.G. Fard, Effect of TiO_2 on phase evolution and microstructure of $MgAl_2O_4$ spinel in different atmospheres, Ceram. Int. 37 (2011) 349-354. https://doi.org/10.1016/j.ceramint.2010.09.016

[22] B. Freudenberg and A. Mocellin, Aluminum titanate formation by solid-state reaction of fine Al_2O_3 and TiO_2 powders, J. Am. Ceram. Soc. 70 (1987) 33-38. https://doi.org/10.1111/j.1151-2916.1987.tb04849.x

[23] B. Ferrari, A. Bartret, C. Baudín, Sandwich materials formed by thick alumina tapes and thin-layered alumina–aluminium titanate structures shaped by EPD, J. Eur. Ceram. Soc. 29 (2009) 1083-1092. https://doi.org/10.1016/j.jeurceramsoc.2008.07.048

[24] N. Montoya, F.J. Serrano, M.M. Reventós, J.M. Amigo, J. Alarcón, Effect of TiO_2 on the mullite formation and mechanical properties of alumina porcelain, J. Eur. Ceram. Soc. 30 (2010) 839-846. https://doi.org/10.1016/j.jeurceramsoc.2009.10.009

[25] Y.F. Zu, G.Q. Chen, X.S. Fu, K.G. Luo, C.G. Wang, S.P. Song, W.L. Zhou, Effects of liquid phases on densification of TiO_2-doped Al_2O_3–ZrO_2 composite ceramics, Ceram. Int. 40 (2014) 3989-3993. https://doi.org/10.1016/j.ceramint.2013.08.049

[26] G.Q. Chen, Y.F. Zu, J.T. Luo, X.S. Fu, W.L. Zhou, Microstructure and superplastic behavior of TiO_2-doped Al_2O_3–ZrO_2 (3Y) composite ceramics, Mater. Sci. Eng. A. 554 (2012) 6-11. https://doi.org/10.1016/j.msea.2012.05.079

[27] A. Kebbede, J. Parai, A.H. Carim, Anisotropic grain growth in α-Al_2O_3 with SiO_2 and TiO_2 additions, J. Am. Ceram. Soc. 83 (2000) 2845-2851. https://doi.org/10.1111/j.1151-2916.2000.tb01642.x

[28] L.H. Xu, Z.P. Xie, L.C. Gao, X.D. Wang, F. Lian, T. Liu, W.C. Li, Synthesis, evaluation and characterization of alumina ceramics with elongated grains, Ceram. Int. 31 (2005) 953-958. https://doi.org/10.1016/j.ceramint.2004.10.008

[29] M. Sathiyakumar and F.D. Gnanam, Influence of additives on density, microstructure and mechanical properties of alumina, J. Mater. Process. Tech. 133 (2003) 282-286. https://doi.org/10.1016/S0924-0136(02)00956-1

[30] X.Y. Teng, H.L. Liu, C.Z. Huang, Effect of Al_2O_3 particle size on the mechanical properties of alumina-based ceramics, Mater. Sci. Eng. A. 452-453 (2007) 545-5511. https://doi.org/10.1016/j.msea.2006.10.073

[31] K. Vishista and F.D. Gnanam, Effect of strontia on the densification and mechanical properties of sol–gel alumina, Ceram. Int. 32 (2006) 917-922. https://doi.org/10.1016/j.ceramint.2005.06.014